International Journal of Renewable Energy Resources 2 (2012) 40-45

ELECTROSPUN METAL OXIDES NANOSTRUCTURES FOR ENERGY RELATED DEVICES

R. Jose,[1] *I.I. Misnon*[1], *P.S. Archana*,[2] *A.L. Viet*,[2] *M.V. Reddy*,[2] *M.M. Yusoff*[1] and *S. Ramakrishna*[1]

[1] Faculty of Industrial Sciences and Technology, Universiti Malaysia Pahang, 26300 Kuantan, Malaysia

[2] National University of Singapore, 117576 Singapore

E-mail: rjose@ump.edu.my; joserajan@gmail.com

ABSTRACT

Metal oxide nanostructures of wide bandgap semiconductors with various morphologies, high degree of crystallinity and surface properties were fabricated by electrospinning a polymeric solution containing respective metal ions and their controlled heat treatment. The metal oxide nanostructures thus developed were tested for their application as charge separation and transport medium in solar cells, cathodes for low voltage (2 V) lithium ion batteries, and super capacitors. The solar cells thus fabricated features enhanced electron diffusion coefficient and energy storage devices featured stable electrochemical cycling thereby making electrospun metal oxide nanostructures a viable product for next generation energy industry.

Keywords: Electrospinning, Metal oxide semiconductors, Dye-sensitized solar cells, lithium ion batteries, supercapacitors

1. INTRODUCTION

One-dimensional (ID) nanostructures are nature's choice when functionalities and flexibilities are to be combined as in extracellular matrices, neural networks, and light harvesting rods of the retina and chlorophyll. Fabrication of one-dimensional structures of the new generation materials could therefore provide new opportunities to improve and/or modify performances of the advanced functional devices and structures. Electrospinning is a process that works under the principle of asymmetric bending of a charged liquid jet when accelerated by a longitudinal electric field. This process has been widely applied to generate nanostructures those are capable to find solutions for immediate requirements such as energy, environment and healthcare (Ramakrishna et al. 2010). The electrospinning technique allows fabrication of continuous nanofibers of polymers and advanced functional materials in a scalable fashion. In this technique, a polymer solution is injected from a needle in the presence of an electric field. When the applied electric field overcomes surface tension of the liquid, a continuous jet is ejected which upon subsequent solvent evaporation and bending produces nanofibers on a collector surface. The electrospinning process and numerous materials and architectures were reviewed by a number of authors; the latest ones can be found elsewhere (Ramakrishna et al. 2010; Teo et al. 2009; Renekar et al. 2008; Ramaseshan et al. 2007; Green et al. 2007). If the polymeric solution contains respective metal ions for formation of an inorganic solid, then annealing such polymeric fibers at desired temperatures would give raise the nanofibrous inorganic solids, which could then be developed in various forms such as nanorods and nanowires. Fig. 1 shows a schematic of the process for the formation of inorganic solid by electrospinning. This paper presents the development of metal oxide nanofibers such as TiO_2, Nb_2O_5, and $SrTiO_3$ for applications in dye-sensitized solar cells, lithium ion batteries, and supercapacitors, respectively.

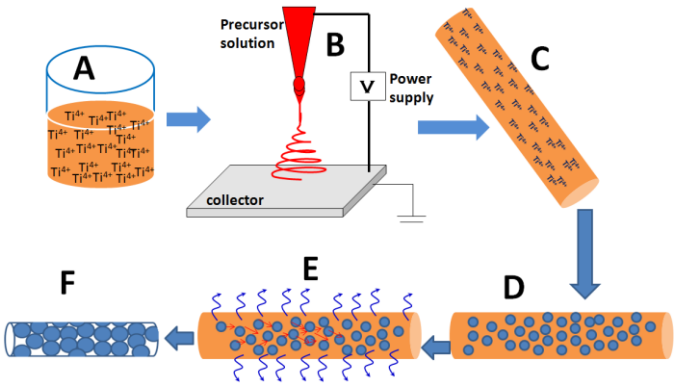

Figure 1: Cartoon showing the steps of process to develop metal oxide nanofibers, TiO_2 as a typical example.

Where: (A) Starting polymeric solution where the ions are dispersed; (B) electrospinning apparatus and procedure; (C) a composite fiber in which titanium ions are dispersed; (D) Heating at a critical temperature leads to a threshold supersaturation for nucleation of TiO_2. Nucleation of the crystals relieves the supersaturation of monomers and the (E) crystal grows from the available monomers, grains undergo a directional mass transport with simultaneous evaporation of polymers and (F) ultimately forms pure inorganic nanofibers. Although the electrospinning is a top-down approach for nanofabrication, the formation of an inorganic species from the polymeric fiber follows bottom-up principles.

2. EXPERIMENTAL PROCEDURE

As shown in Fig. 1, synthesis of nanofibers by electrospinning starts by preparing a polymeric solution of optimum viscosity which duly dispersed with

respective metal ions. In the present study, polyvinylpyrrolidone (PVP; Mw = 1,300,000, Sigma-Aldrich) was chosen as the polymer. All the electrospinning was performed in a commercial electrospinning set-up (NANON) at accelerating voltages 20-30 kV at humidity ≤50% at a flow rate of 0.5-2 ml/h. The composite fibers containing the metal ions in PVP were collected either on a rotating drum or on a flat surface wrapped with an aluminum foil.

2.1 Synthesis of TiO_2

Details of synthesis of TiO_2 can be found in our previous publication (Kumar et al. 2007). Briefly, the TiO_2 sol was prepared by hydrolyzing 0.25 gm of titanium tetraisopropoxide [$Ti(OiPr)_4$; 97%, Sigma-Aldrich] with a mixture of 1 ml of ethanol (98%) and 1 ml of acetic acid (100%, BDH, AnalaR). Next, the PVP (~9 wt%) was separately dissolved in ~2.75 ml of ethanol and then added to the TiO_2 sol solution. The precursor mixture was stirred for 12 hours at room temperature to attain sufficient viscosity required for electrospinning. The as-spun PVP-TiO_2 composite nanofibers were then annealed at ~120 ^oC for 12 h for drying and removal of solvents. The annealed fibers were then sintered in the range 450 – 650 ^oC for 30 min.

2.2 Synthesis of Nb_2O_5

PVP, ethanol, niobium ethoxide (99.95% trace metals basis, Sigma Aldrich), and acetic acid were the starting materials. Niobium ethoxide (0.5 g) and PVP (0.3 g) were added to a solution of ethanol (3.5 ml) and acetic acid (1 ml). The solution was stirred in an airtight bottle for 24 h and obtained a clear solution. The composite fibers were annealed at 500, 800, 1000, and 1100 °C for 1h in air in a carbolyte box furnace. Details of synthesis are in our previous publications (Anh et al. 2010, Anh et al. 2011).

2.3 Synthesis of $SrTiO_3$

Strontium acetate (mol wt: 205.71), acetic acid, trifluroacetic acid, titanium tetraisopropoxide [$Ti(iPr)_4$] PVP (Mw=1,300,000), and ethanol were used as starting materials. The strontium acetate (1.275 g) was dissolved in acetic acid (5 ml) and stirred for 90 min. A precipitate was observed which was dissolved by trifluroacetic acid (0.4 g) under continuous stirring. The resulting solution was mixed with a solution containing PVP (0.32 g) in ethanol (3 ml). The $Ti(iPr)_4$ (1.74 g) was added dropwise under continuous stirring. The fibers were annealed at 900 ^oC for 2 h to synthesize $SrTiO_3$ phase based on the thermal analyses results.

2.4 Characterization

Crystal structures of the annealed fibers were studied by x-ray and electron diffraction techniques. The x-ray diffraction (XRD) patterns were recorded by x-ray diffractometer (Philips, X'PERT MPD, CuKα radiation). Lattice parameters were calculated using TOPAS software by fitting the observed XRD patterns to the respective crystal structure. Morphology, surface, and crystal structure of the samples were studied by scanning electron microscopy (SEM; Quanta 200 FEG System: FEI Company, USA) and transmission electron microscopy (TEM; JEOL 2010Fas). The Brunauer-Emmett-Teller (BET) surface area of the fibers was measured by a surface area analyzer (Micromeritics Tristar 3000). The fiber densities were determined by using a pycnometer (AccuPyc 1330, Micromeritics). X-ray photoelectron spectra (XPS) of the Nb_2O_5 nanofibers were obtained using a VG Scientific ESCA MK II spectrometer with monochromatic Mg-K_α radiation (1253.6 eV). Details of XPS measurements are in our previous publication (Anh et al 2010).

3. RESULTS AND DISCUSSION

3.1 Dye-sensitized solar cells

The dye-sensitized solar cells (DSCs) have emerged as one of the low-cost photovoltaic device due to less fabrication cost and less-expensive raw materials. The photovoltaic effect in DSCs occurs at the interface between a dye-anchored wide bandgap nanostructured metal oxide semiconductor (n-MOS) and a redox electrolyte (Grätzel 2005). Intensity of solar light is weak at the absorption wavelength window of most MOSs, which is conventionally widened by sensitizing by organic flourophores (dyes), hence the name dye-sensitized solar cells. On sunlight irradiation, the dye absorbs solar light thereby creates a transiently localized state called exciton. The exciton can be viewed as a quasi particle composing an (e^-–h^+) pair. If the conduction band energy of the MOS is at lower energies than the lower unoccupied molecular orbital (LUMO) of the dye, then the excited electron decays to the MOS and thereby creating mobile charge carriers (Jose et al. 2009; Yella et al. 2011). The electrons injected to the conduction band of the MOS is transported through the mesoporous network to the counter electrode by doing a work equal to the energy difference between the conduction band energy of the electrode and redox potential energy of the electrolyte. The oxidized dye is regenerated by a hole-conductor, thereby completing the cycle of operations. Research over the past decade brought the photoelectric conversion efficiency (η) of DSCs to 12% (Yella et al. 2011). The state-of-the art DSC uses a mesoporous TiO_2 particles sensitized by an organic sensitizer and copper iodide-based electrolyte (Yella et al. 2011).

All the three metal oxides synthesized here, viz. TiO_2, Nb_2O_5, and $SrTiO_3$ were used for fabricating DSCs. The electrodes were prepared as described before (Anh et al 2010, ; Archana et al, 2011; Archana et al 2009; Naveen et al. 2012; Jose et al 2008; Jose et al 2009 Fujihara et al 2007; Mukherjee et al. 2009). The TiO_2 nanorod electrodes (area ~1 cm^2) were soaked in a 1:1 vol. mixture of acetonitrile and *tert*-butanol with ruthenium dye ($RuL_2(NCS)_2$-$2H_2O$; L=2.2'-bipyridyl-4,4'-dicarboxylic acid (0.5 mM, N3 Solaronix) for 12 h at room temperature. The soaked electrodes were washed with ethanol to remove non-anchored dye molecules and then dried in the air. Pt sputtered FTO glasses were used as counter electrode. The Pt counter electrode and the dye anchored TiO_2 electrode were assembled into a sealed sandwich type cell using a sealing material (SX1170-25, film thickness = 25 μm, Solaronix). Acetonitrile containing 0.1M lithium iodide, 0.03M iodine, 0.5M 4-*tert*-butylpyridine, and 0.6M 1-propyl-2,3-dimethyl imidazolium iodide was used as redox electrolyte solution. The electrolyte solution was injected into the cell through a small opening drilled on the

counter electrode. Finally the opening was sealed by a piece of glass. Current-voltage characteristics and electrochemical impedance spectroscopy (EIS) data were obtained using a potentiostat (Autolab PGSTAT30, Eco Chemie B.V., The Netherlands). The EIS measurements were carried out in the dark using 10 mV ac voltage superimposed on a forward-biased DSC (0.4–0.7 V) with frequency ranging from 30 kHz to 0.05 Hz. The electron transport was also studied using transient photocurrent technique, the details of which are available in our earlier publications (Archana et al. 2009; Archana et al 2010). Figure 2 shows the cross-sectional SEM image of the TiO_2 nanofiber based cell after measuring the I-V characteristics. The films were of uniform thickness of ~13 – 15 µm, which was further confirmed by thickness profilometry. The white dots in the images are the electrolytes dried up after measurement which indicate good permeation of electrolyte within the volume of the cells. Table 1 shows the photovoltaic parameters of the various TiO_2 devices used in this study. The electrospun TiO_2 based devices showed only 50% performance of that of the nanoparticle based device.

Table 1: Photovoltaic properties of the electrospun TiO_2 and Nb_2O_5 based devices. J_{SC} – Current density; V_{OC} – Open circuit voltage; FF – Fill Factor; η – Efficiency

Morphology	J_{SC} (mA/cm^2)	V_{OC} (V)	FF (%)	η (%)
TiO_2 Fibers	9.45	0.78	57	4.2
TiO_2 rods	13	0.83	49	5.2
TiO_2 wires	8.46	0.82	60	4.3
TiO_2 NPs (Wang et al 2006)	17.05	0.86	76	11
H-Nb_2O_5	6.68	0.77	59	3.1
$SrTiO_3$	5.5	0.67	43	1.6

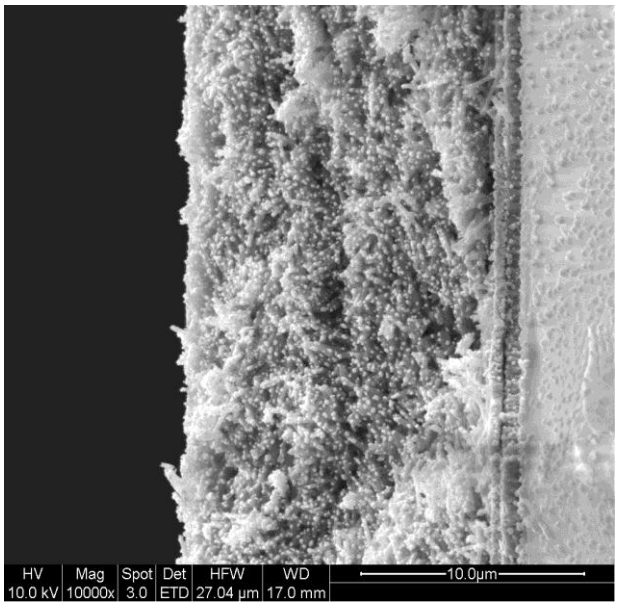

Figure 2: Cross-sectional SEM image of a nanowire based device after fabricating DSCs. The white spot like feature is the dried electrolyte.

The superior performances of the nanoparticles device result from their higher surface area (≥ 100 m^2/g) as well as various scattering and hole blocking layers compared to that of the electrospun nanostructures (≤ 50 m^2/g). One of the main focuses in these studies were to quantify the electron diffusion coefficient (D_n) through the random arrangement of one-dimensional nanostructure network. In DSCs, the distance travelled by electrons before recombining with the electrolyte, known as diffusion length is a crucial parameter. The diffusion length is given by $L = (D_n \tau)^{1/2}$, where τ is the electron lifetime. As mentioned before, τ is ~10^{-6} s, which limits the diffusion length to be several microns assuming the D_n to be 10^{-4} cm^2/s. For efficient charge collection in DSCs, the thickness of the mesoporous metal oxide electrode should be one-third of the diffusion length. Therefore, the poor D_n of the nanocrystalline metal oxide semiconductors intrinsically limits the photovoltaic conversion efficiency. Our experiments demonstrate that electrospun random network fabricated on conducting glass plates have at least an order of magnitude higher D_n compared to the corresponding nanoparticles (Archana et al. 2009; Archana et al. 2010; Archana et al. 2011). Fig. 3 shows the D_n measured by transient photocurrent measurements of electrospun TiO_2 nanowires with and without increasing the crystallinity through additional heat treatment, which shows improved D_n for the electrospun nanowires compared to nanoparticles for similar photoexcitation density. The enhanced D_n provides opportunities for fabricating high performance DSCs.

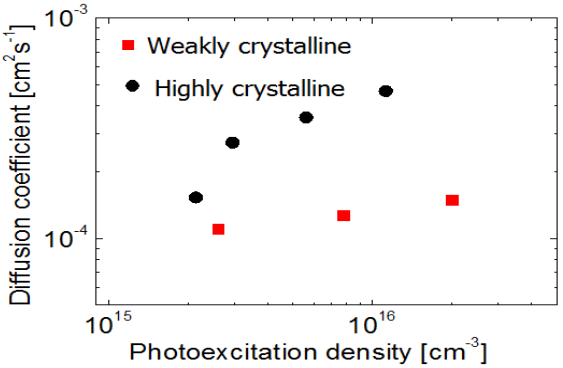

Figure 3: The electron diffusion coefficient as a function of photoexcitation density measured using transient photocurrent measurement (Archana et al. 2009).

3.2 Lithium ion battery

The renewable energy is a dual topic of energy conversion and storage. Many electrochemical devices that integrate different energy storage modes have been investigated in recent years for reversible energy storage, a brief account of which is available in recent reviews (Armand et al. 2008; Grätzel 2001; Tarascon et al. 2001). The intercalation storage of lithium ions is widely used due to its potentially large operational voltage window, high energy density, fast power capability, safety, and long cycle life. Conventional lithium ion battery (LIB) consists of $LiCoO_2$ (cathode), graphite (anode), and a non-aqueous Li- ion conducting electrolyte. The lithium ion is inserted in the anode from the cathode (intercalation) during the charge cycle and vice versa

during the discharge cycle (deintercalation) due to the electrochemical reactions happening at the respective electrodes. Nanostructured materials come into picture due to their high specific surface area which will enable to absorb the volume changes due to the smaller number of atoms in the nano-grains of the electrodes. Also, an increased access of Li to the alloy-forming metal particles and short diffusion path length for Li-ions will enable improved electrode kinetics, solid electrolyte interphase formation, and current-rate capability (Bruce et al. 2008).

Electrodes for the electrochemical studies were prepared by mixing the metal oxide nanofibers with carbon black and polyvinylidene fluoride copolymer (binder, Kynar 2801) with ratio 65:20:15 and 70:15:15. N-methyl 2-pyrrolidinone was used as the solvent to disperse the nanofibers, carbon black, and the binder. The doctor Blade technique was used to deposit a ~20 µm thick layer of the prepared slurry on an etched copper foil. Circular electrode (area ~2 cm^2) was cut from the coated copper foil. Electrode heat treatment play an important role on lithium battery performances; therefore, some electrodes were further heated at 220 °C in Argon gas for 6 h to improve the contact between Cu-current collector, conducting carbon, active material, and PVDF binder. Glass microfiber filter (Whatman) membrane was used as separator. The counter and reference electrodes were a circular piece of lithium metal of area ~2 cm^2. Coin-type test cells (CR2016) were fabricated in an Ar-gas filled glove box. Cyclic voltammetry and discharge-charge cycling were carried out using Mac-pile II (Bio-logic, France), bitrode battery tester (Model SCN, USA), respectively.

All the electrospun fibers polymorphs showed good cycling stability; however, the specific capacities differed considerably depending on the crystal structure (Anh et al. 2010; Anh et al 2010). The monoclinic Nb_2O_5 (M-Nb_2O_5) showed highest capacity (~240 $mAhg^{-1}$) among all the phases considered in the present study. The M-Nb_2O_5 phase also showed the lowest capacity fading among all the phases. It was also demonstrated from the specific capacity and cycling stability of M-Nb_2O_5 annealed at different temperatures that incomplete phase formation or highly defective crystalline structure adversely affects lithium intercalation/de-intercalation behavior both in terms of specific capacity and cycling stability. The observed stability is thought to arise from the peculiar porous structure of electrospun nanofibers that helps complete desorption of the lithium ions during the discharge cycle. The results of the present study indicate that electrospun M-Nb_2O_5 nuggets could be an excellent candidate for rechargeable 2 V lithium batteries in view of the commercial viability of the electrospinning process and performance of the batteries developed herewith.

3.3 Supercapacitors

Supercapacitors or electrochemical double layer capacitors, which store energy electrostatically by reversible adsorption of ions in an electrolyte onto electrodes, have gained considerable attention as an energy storage device due to their high energy density compared to the common electrolytic capacitors (Simon and Gogotsi, 2008). Charge separation in the supercapacitors occurs on polarization at the electrode – electrolyte interface, producing the double layer capacitance. The electrode materials should be electrochemically stable for safe operation in an extended period of time and should have high surface area for large specific capacitance (Simon and Gogotsi, 2008). Supercapacitor devices were fabricated by dispersing 75 wt% the electrospun $SrTiO_3$ fibers, 20 wt% Super P, and 5 wt% polyvinylidene fluoride in N-methyl pyrrolidone solvent pasted on graphite paper substrate. The mass per unit area of the electrode was kept constant at 5 mg/cm^2. The electrodes were dried at 60 ^oC for 4 h. All the electrochemical measurements were carried out by using a SI 1255B Frequency response analyzer. Electrochemical measurements such as cyclic voltammetry (CV) and galvanostatic charge/discharge were carried out in two electrode geometry in 1M H_2SO_4 electrolyte. Cyclic voltammograms were recorded in the potential range from -0.2 to 0.8 V at scan rates of 5, 10, 20 and 50mV/s. Galvanostatic charge/discharge cycling was performed over the voltage range from 0-1V at the current density of $1mA/cm^2$.

Fig. 4 shows the CV of $SrTiO_3$ electrospun fibers coated on graphite electrode recorded in 1M H_2SO_4 by cycling continuously the electrode potential between -0.2 to 0.8 V at different scan rates. No clear peak was observed voltammograms in the -0.2 to 0.8V range at all scan rates. The measured CVs were very close to rectangular shape which is the characteristic of an ideal double-layer capacitor. The specific capacitances (Cs) calculated from cyclic voltammograms were 37, 24, 24 and 6.5 F/g at the scan rate of 5, 10, 20 and 50 mV/s, respectively. i.e., the Cs decreases when scan rate increases. One possible reason for the lowered specific capacitance compared to successful supercapacitors such as RuO_2 (Cs ~600 F/g) (Simon and Gogotsi, 2008) is the lower specific surface area of the materials used for measurements here. Stability of the supercapacitive behavior was evaluated from the current densities from CV measurements vs. scan rates (Figure 3). A linear increase in the current densities with scan rate was observed indicating stable supercapacitive characteristics of the $SrTiO_3$ electrospun fibers.

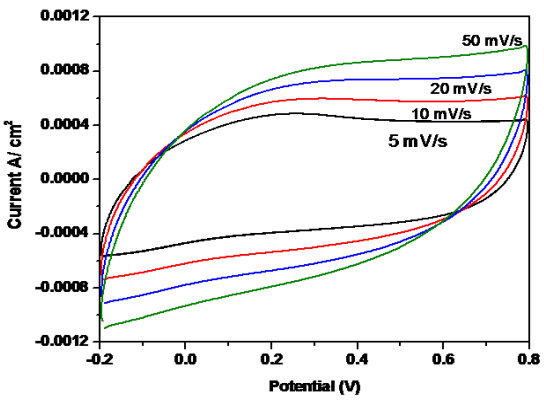

Figure 4: Cyclic voltammograms of SrTiO3 electrospun fibres at different scan rates recorded in 1M H_2SO_4

Fig. 5 shows galvanostatic charge/discharge behavior of $SrTiO_3$ electrospun fibers at current density of 1mA/cm^2. It can be seen that, the charge curves are somewhat mirror symmetrical to their discharge counterparts in the whole potential range. The Cs was calculated using the formula (Ghenaatian et al. 1998):

$$C_S = \frac{2I}{m.dV/dt}$$

where, I is the applied current density, m is the mass of active material and dV/dt is the slope of discharge curve. The Cs calculated from the galvanostatic cycles was ~33.33F/g, which is comparable with the value measured from CV. To summarize, measured cyclic voltammograms of $SrTiO_3$ fibers showed ideal stable supercapacitive characteristics, although absolute value of specific capacitance is rather low. Mesoporous $SrTiO_3$ particles with high specific surface area could be a material of choice as an energy storage medium.

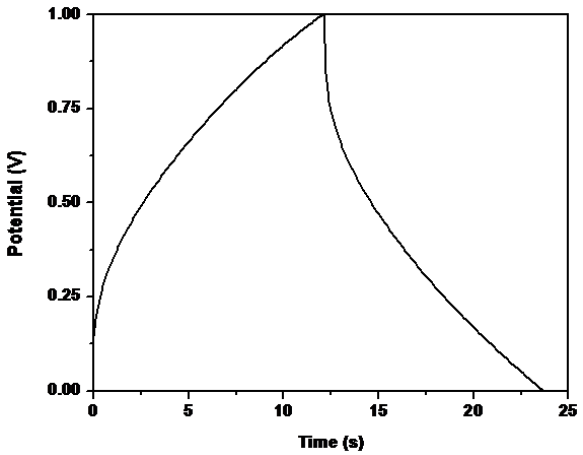

Figure 5: Galvanostatic charge/discharge of SrTiO3 electrospun fibers at a current density of 1mA/cm^2

4. CONCLUSIONS

Electrospinning has emerged as a scalable nanofabrication technique for a number of materials systems including polymers, polymer-nanocomposites, metals, metal oxides, nitrides, and carbides. They combine a number of physical properties such as guided electron transport; strain induced electronic properties, high mechanical strength, high degree of flexibility, large specific surface area, high electron and thermal diffusivity, and tailorable pore distribution. Owing to the never ending need for cleaner energy, water, and regenerative medicine, electrospun nanofibers are used globally to find solutions for these issues. The guided electron transport, availability of space charge depleted space charge region, and enhanced electron diffusivity of electrons were utilized to fabricate dye-sensitized solar cells with high photoelectric conversion efficiency in limited number of fabrication steps. Similar efficiencies were achieved otherwise, for e.g., using nanoparticles, involved complex multi-step processes. Peculiar pore size distribution and tailorable crystallinity made electrospun nanofiber based lithium ion batteries and supercapacitors to perform longer durations without appreciable loss of capacity. These unique properties would provide electronspun metal oxide nanostructures as a viable product for next generation energy industry.

5. ACKNOWLEDGEMENTS

Authors would like to acknowledge the Research and Innovation Department, Universiti Malaysia Pahang (RDU100377) as well as Fundamental Research Grant Scheme (RDU 110103) for supporting this project.

REFERENCES

Archana, P. S., R. Jose, Jin, T.M., Vijila, C., Yusoff. M. M., Ramakrishna, S. 2010. Structural and electrical properties of Nb-doped anatase TiO2 nanowires by electrospinning, Journal of the American Ceramic Society 93(12): 4096-4102.

Archana, P. S., R. Jose, Vijila, C., Ramakrishna, S. 2009. Improved electron diffusion coefficient in electrospun TiO_2 nanowires, Journal of Physical Chemistry C 113: 21538-21542.

Archana, P. S., R. Jose, Yusoff, M. M., Ramakrishna, S. 2011. Near Band Edge electron diffusion in electrospun Nb-doped anatase nanofibers probed by electrochemical impedance spectroscopy, Applied Physics Letters 98: 152106.

Armand, M., Tarascon, J. M. 2008. "Building better batteries." Nature 451(7179): 652-657.

Bruce, P. G., Scrosati, B., Tarascon, J. M., 2008. Nanomaterials for rechargeable lithium batteries, Angewandte Chemie-International Edition 47(16): 2930-2946.

Daeneke, T., Kwon, T. H., T. H.; Holmes, A. B.; Duffy, N. W.; Bach, U.; Spiccia, L., 2011. High-efficiency dye-sensitized solar cells with ferrocene-based electrolytes, Nature Chemistry 3(3): 211-215.

Fujihara, K., Kumar, A., Jose, R.; Ramakrishna, S.; Uchida, S., 2007. Spray deposition of electrospun TiO2 nanorods for dye-sensitized solar cell, Nanotechnology 18(36): 365709.

Ghenaatian, H. R., Mousavi, M. F., Rahmanifar, M.S. 1998. High performance battery-supercapacitor hybrid energy storage system based on self-doped polyaniline nanofibers, Synthetic Matals 93: 2017-2023.

Gratzel, M. 2001. Photoelectrochemical cells. Nature 414(6861): 338-344.

Grätzel, M. 2005. Solar Energy Conversion by Dye-Sensitized Photovoltaic Cells, IInorganic Chemistry 44(20): 6841-6851.

Green, M. A., Emery, K., King, D. L., Hoshikawa, Y., Warta, W. 2007. Solar Cell Efficiency Tables (Version 29), Progress in Photovoltaics: Research and Application 15: 35-40.

Jose, R., A. Kumar, Thavasi, V. Fujihara, K., Uchida, S., Ramakrishna, S. 2008. Relationship between the molecular structure of the dyes and photocurrent density in the dye-sensitized solar cells, Applied Physics Letters 93: 023125.

Jose, R., A. Kumar, Thavasi, V. Fujihara, K., Uchida, S., Ramakrishna, S. 2008. Conversion

efficiency versus sensitizer for electrospun nanofibers for the dye-sensitized solar cells, Nanotechnology 19: 424004.

Jose, R., Thavasi, V., Ramakrisha, S. 2009. Metal Oxides for dye-sensitized solar cells Journal of the American Ceramic society 92(2): 289-301.

Kumar, A., Jose, R., Fujihara, K., Wang, J., Ramakrishna, S. 2007. Structural and optical properties of electrospun TiO_2 nanofibers, Chemistry of Materials 19: 6536-6542.

Le Viet, A., R. Jose, et al. (2010). Nb2O5 photoelectrodes for dye-sensitized solar cells: Choice of the polymorph, Journal of Physical Chemistry C 114(49): 21795-21800.

Le Viet, A., M. V. Reddy, Jose, R., Chowdari, B. V. R., Ramakrishna, S. 2010. Nanostructured Nb2O5 Polymorphs by Electrospinning for Rechargeable Lithium Batteries, Journal of Physical Chemistry C 114: 664-671.

Le Viet, A., M. V. Reddy, Jose, R., Chowdari, B. V. R., Ramakrishna, S. 2011. Electrochemical properties of bare and Ta-substituted Nb2O 5 nanostructures, Electrochimica Acta 56(3): 1518-1528.

Mukherjee, K., T. H. Teng, Jose, R., Ramakrishna, S., 2009. Electron transport in electrospun TiO2 nanofiber dye-sensitized solar cells, Applied Physics Letters 95(1): 012101.

Naveen Kumar, E., R. Jose, Archana P. S., Vijila, C, Yusoff, M. M., Ramakrishna, S. 2012. High performance dye-sensitized solar cells with record open circuit voltage using tin oxide nanoflowers developed by electrospinning, Energy and Environmental Science Sci. 5: 5401-5407

Ramakrishna, S., Jose, R., Archana, P. S., Nair, A. S., Balamurugan, R., Venugopal, J. R., Teo, W. E. 2010. Science and Engineering of Electrospun Nanofibers for Advances in Clean Energy, Water Filtration, and Regenerative Medicine, Journal of Materials Science 45: 6283-6312.

Ramasheshan, R., S. Sundarrajan, Jose, R., Ramakrishna, S. 2007. Nanostructured ceramics by electrospinning, Journal of Applied Physics 102(12): 111101.

Reddy, M. V., Jose, R., Teng, T. H., Chowdari, B. V. R., Ramakrishna, S.. Electrochimica Acta 55: 3109-3117.

Reneker, D. H. and Yarin A. L. 2008. Electrospinning jets and polymer nanofibers, Polymer 49: 2387-2425.

Simon, P. and Gogotsi, Y. 2008. Materials for electrochemical capacitors, Nature Materials 7: 845-854.

Tarascon, J. M. and Armand, M. 2001. Issues and challenges facing rechargeable lithium batteries Nature 414 (6861): 359-367.

Teo, W. E. and Ramakrishna, S. 2009. Electrospun nanofibers as a platform for multifunctional, hierarchically organized nanocomposite, Composites Science and Technology 69: 1804-1817.

Wang, Q., S. Ito, S.; Grätzel, M., Fabregat-Santiago, F., Mora-Sero, I., Bisquert, J., Bessho, T., Imai, H. 2006. Characteristics of high efficiency dye-sensitized solar cells, Journal of Physical Chemistry B 110(50): 25210-25221.